Isobutanol-Methanol Mixtures from Synthesis Gas

Quarterly Technical Progress Report

Period Covered: 1 April to 30 June 1996

Contractor

University of California-Berkeley
Berkeley, California 94720

Enrique Iglesia - Program Manager

25 July 1996

Prepared for the United States Department of Energy *
Under Contract Number DE-AC22-94PC94066
Contract Period 1 October 1994 - 30 September 1997

DISCLAIMER

TABLE OF CONTENTS

EXECUTIVE SUMMARY

A series of $CuMgCeO_x$ catalysts have been prepared by coprecipitating the corresponding metal nitrates with a mixed solution of potassium carbonate and potassium hydroxide. The bulk composition of the catalyst has been measured by atomic absorption (AA) analysis and the Cu dispersion has been determined by N_2O titration at 90 °C. A $^{13}CO_2/^{12}CO_2$ exchange method provides a direct measure of basic site density and strength at reaction conditions. Addition of K to Cu-Mg-CeO_x increases both basic site density and strength, but decreases Cu dispersion (as determined by N_2O titration).

Kinetic studies of methanol and ethanol coupling reactions on K-Cu/MgO/CeO_2 and MgO/CeO_2 catalysts indicate that Cu enhances the rates of alcohol dehydrogenation. The cross-coupling reactions of acetaldehyde and ^{13}C-labeled methanol produce singly-labeled propionaldehyde, suggesting that it forms by the condensation of acetaldehyde and a reactive intermediate derived from methanol. Isobutyraldehyde, a precursor to isobutanol, forms via the condensation of propionaldehyde and a reactive C_1 intermediate resulting from methanol. CO_2, one of the reaction products, poisons both basic and metal sites on Ce-containing $CuMgO_x$ catalysts, resulting in decreases in the rates of both alcohol dehydrogenation (Cu sites) and chain-growth condensation reactions (basic sites). CO_2 inhibits ethanol dehydrogenation on both low-Cu and high-Cu $CuMgCeO_x$ catalysts; however, CO_2 has no effect on the activity of low-Cu Ce-free Cu-MgO_x catalysts, suggesting that the Cu on $CuMgCeO_x$ catalysts is more likely to be oxidized by CO_2 to Cu^+ species that can be subsequently stabilized by CeO_2.

CO_2 effects on high-pressure isobutanol synthesis from CO/H_2 have been studied on low- and high-Cu $CuMgCeO_x$ catalysts at 320 °C and 4.5 MPa. CO_2 addition and removal on low- and high-Cu catalysts show similar directional effects on CO conversion. CO conversion is lower at all space velocities in the presence of CO_2, and removal of CO_2 from the feed partially recovers CO conversion. CO_2 decreases methanol and isobutanol productivities on both catalysts. Addition of 1-propanol to CO/H_2 feed increases isobutanol production, suggesting that 1-propanol is a precursor to isobutanol.

In-situ IR studies of preadsorbed ethanol on MgO show three types of ethoxide species as evidenced by three C-O stretching bands in the 1000-1200 cm^{-1} region. The C-O band at 1108 cm^{-1} decreases dramatically as temperature increases from 25 to 100 °C, suggesting that it corresponds to weakly adsorbed ethanol. The other two C-O bands do not disappear until the temperature reaches 300 °C. The decrease in the ratio of band 2925 cm^{-1} (CH_2 group) to band 2968 cm^{-1} (CH_3 group) with increasing temperature suggests that ethoxide species undergoes dehydrogenation reaction leading to the formation of surface acetate. The bands in the 1300-1600 cm^{-1} region at high temperatures are attributed to surface acetate and carbonate species. At temperatures greater than 300 °C, surface ethoxide and acetate species no longer exist, as shown by the disappearance of C-H stretching bands. Dehydroxylation reactions at elevated temperatures lead to the formation of isolated hydroxyl species on MgO surface.

1. CONTRACT OBJECTIVES AND TASKS

The contract objectives are:

1. To design a catalytic material for the synthesis of isobutanol with a productivity of 200 g isoalcohols/g-cat-h and a molar isobutanol-to-methanol ratio near unity

2. To develop structure-function rules for the design of catalysts for the selective conversion of synthesis gas to isoalcohols

The research program has been grouped into five specific tasks and a set of project management and reporting activities. The abbreviated designations for these tasks are:

- Project Work Plan ***(Task 1)***

- Catalyst Synthesis ***(Task 2)***

- Catalyst Evaluation in Laboratory Scale Reactors ***(Task 3)***

- Identification of Reaction Intermediates ***(Task 4)***

- Bench-Scale Catalyst Evaluation at Air Products and Chemicals ***(Task 5)***

2. SUMMARY OF ACTIVITIES

Activities during this period have focused on:

- Preparation of a series of K-Cu/MgO/CeO_2 and Cs-Cu/ZnO/Al_2O_3 catalysts

- Determination of basic site density and strength at reaction conditions using $^{13}CO_2/^{12}CO_2$ switch methods

- Isotopic tracer studies of alcohol coupling reactions on MgO/CeO_2-based copper catalysts

- Evaluation of high-pressure isobutanol synthesis reactions using K-Cu/MgO/CeO_2 catalysts

- Determination of CO_2 effects on K-Cu/MgO/CeO_2 and Cs-Cu/ZnO/Al_2O_3 catalysts

- *In-situ* IR studies of pre-adsorbed ethanol on MgO

3. STATUS, ACCOMPLISHMENTS, AND RESULTS

Task 1: Management Plan

No activities were carried out during this reporting period.

Task 2: Catalyst synthesis

Cu-Ce-Mg samples were prepared by coprecipitation of 1 M mixed metal nitrate solutions with a mixed solution of potassium hydroxide (2M) and potassium carbonate (1M) at 65°C and a constant pH of 9 in a computer-controlled well-stirred batch reactor. The precipitates were filtered, washed with distilled water at 65°C, and then dried at 80-90°C overnight. The resulting materials were calcined at 450°C for 4 h to obtain the mixed oxides. The detailed procedures have been described by Apesteguia et al. [1]. K-promoted $Cu/MgO/CeO_2$ samples were prepared by incipient wetness impregnation of $Cu/MgO/CeO_2$ with K_2CO_3 (0.25 M) solution, followed by dryness and calcination. Catalyst properties are summarized in Table 1.

Table 1. Composition and surface areas of catalytic oxides.

Sample	Mg/Cu	Mg/Ce	K (wt.%) nominal	K (wt.%) AAS	S.A. (m^2 / g)	Cu S.A. (m^2 / g)
MG 3 - 6 O	0.7	4.9	< 0.01	1.9	65	7.4
MG 3 - 6 Ow	0.7	4.9	< 0.01	0.03	117	
MG 3 - 6 Ow/K	0.7	4.9	1.0	1.2	92	21.9
MG 3 - 11 O	9.6	4.7	<0.01	2.6	93	5.4
MG 3 - 11 O/K	9.6	4.7	1.0	3.5	61	4.6
MG 3 - 11 Ow	9.6	4.7	<0.01	0.1	167	17.2
MG 3 - 11 Ow/K	9.6	4.7	1.0	0.9	147	10.4
MG 3 - 2 O		4.6	<0.01	5.3	53	
MG 3 - 4 O			<0.01		1.5	
MG 3 - 7 O		5.2	<0.01	0.03	188	
MG 3 - 8 O			<0.01	0.2	194	

BET surface areas (S_g) were measured by nitrogen adsorption at 77 K. The bulk composition of the sample was determined by atomic absorption (AA) spectroscopy. The atomic ratios of Mg/Cu and Mg/Ce are in good agreement with the values calculated from the starting precursors. The difference between the nominal and the actual K concentrations on $Cu/MgO/CeO_2$, MgO/CeO_2 and MgO are due to the inability of removing K during the washing step. The surface area was found to decrease with increasing K-loading. Lunsford and co-workers [2,3] have reported that the addition of Li to MgO results in a decrease in MgO surface area due to sintering.

Copper surface area was determined by Cu surface atom titration at 90 °C using N_2O introduced by pulse injection. The detailed experimental procedures were described

in the previous quarterly report [4]. Cu surface area decreased with increasing K-loading because of a decrease in $MgCeO_x$ surface area and possibly also because K-species block surface Cu atoms, resulting in a lower number of exposed surface Cu atoms (Table 1) [5].

MG3-6 O ($Cu_{7.5}Mg_5CeO_x$) and MG3-11 O ($Cu_{0.5}Mg_5CeO_x$) contained large amounts of K, left behind during co-precipitation (Table 1). The MG3-6 and MG3-11 O precursor materials were re-washed in 1000 mL deionized water at 65 °C for 30 min in a stirred-batch reactor. The resultant precipitates were filtered, washed with 600 mL deionized water and calcined to give the mixed oxides MG3-6 Ow and MG3-11 Ow, respectively. MG3-6 Ow and MG3-11 Ow were impregnated with potassium by incipient wetness using a K_2CO_3 solution to give the corresponding MG3-6 Ow/K and MG3-11 Ow/K catalysts. The nominal potassium addition was 1 wt.%. The samples were re-calcined at 450 °C for 4 h. Their properties are summarized in Table 1.

Due to the high concentrations of residual potassium left behind during co-precipitation on MG3-2 O (Mg_5CeO_x) and MG3-4 O (MgO) (Table 1), a new batch of each material was synthesized. They were designated as MG3-7 O and MG3-8 O, respectively. Atomic analysis results showed less residual K on these samples because of better washing. The total surface area increased dramatically upon the removal of K (Table 1).

During this reporting period, Cs-$CuO/ZnO/Al_2O_3$ catalysts were also synthesized. Samples were prepared by co-precipitation of 1 M mixed metal nitrate solutions with Na_2CO_3 (1 M) at 65 °C and with a pH of 7 in a well stirred-batch reactor. The precipitates were filtered, *washed thoroughly* with deionized water at 65 °C to remove K, and dried at 80-90 °C overnight. The resulting precursors were calcined at 350°C for 4 h to obtain the mixed metal oxides. Catalyst compositions and surface areas are given in Table 2. Powder X-ray diffraction (XRD) was used to determine the phases present in the mixed oxides. These mixed metal oxides will be subsequently impregnated with Cs by incipient wetness impregnation with cesium acetate solution.

Table 2. Composition and surface areas of Cu/Zn/Al catalytic oxides.

Sample	**M_xO_y (wt.%)**				**S.A.**	**Identified**
	Cu	**Zn**	**Al**	**Na**	(m^2 / g)	**compound** (XRD)
MG 4 - 1 O	26.7	56.9	15.1	0.3	99	CuO, ZnO
MG 4 - 2 O	55.1	31.0	9.7	0.1	76	CuO, ZnO
MG 4 - 3 O	-----	91.2	7.8	0.1	146	ZnO

Task 3: Catalyst Evaluation in Laboratory Scale Reactors

3.1 Kinetic Studies of Alcohol Coupling Reactions

Alcohol coupling reactions consist of a sequence of steps leading to the formation of higher alcohols from C_1 and C_2 alcohols [6, 7]. These steps include alcohol

dehydrogenation to aldehydes, aldol condensation of aldehydes to higher oxygenates, and their subsequent hydrogenation to alcohols. It is believed that aldehydes are the reactive intermediates in chain-growth reactions that occur on basic sites [7, 8].

Ethanol dehydrogenation-coupling reactions were previously reported for K-Cu-Ce-Mg catalysts [4]. Ethanol is a useful and simple probe molecule to test the metal and basic functions of isobutanol synthesis catalysts. Ethanol reactions, however, lead only to acetone and n-butyraldehyde (precursors to 2-propanol and 1-butanol, respectively), neither of which can form isobutanol precursors (e.g. isobutyraldehyde, propionaldehyde) during CO hydrogenation (Figure 1).

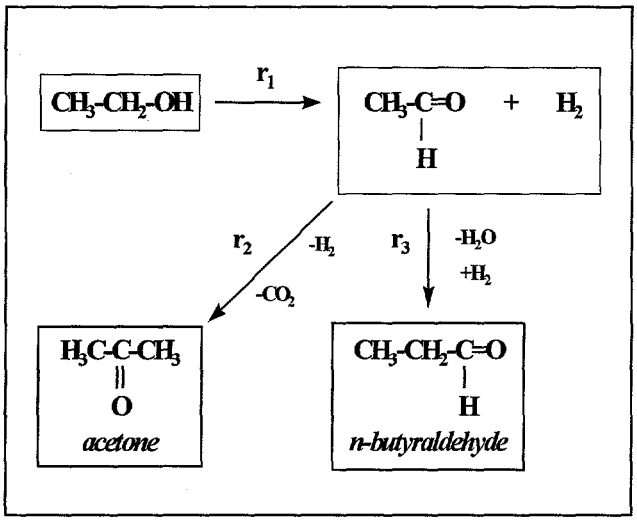

Figure 1. Reaction scheme for ethanol reactions.

^{13}C-tracer studies of methanol-acetaldehyde cross-coupling reactions were carried out in order to examine chain growth reaction pathways leading to C_3 oxygenates. In a typical experiment, 22 mg of catalyst was charged into a gradientless batch reactor. The sample was reduced in 10 % H_2 (balance He) at 350 °C for 30 min. After the desired reaction temperature was reached, reactants were fed to the reactor. For the coupling reaction of methanol and acetaldehyde on $Cu/MgO/CeO_2$ and MgO/CeO_2, the feed gas composition was $C_2H_4O/^{13}CH_3OH/CH_4/He$ = 4.0/8.0/2.7/86.6 kPa (methane was used as an internal standard). The reaction was carried out at 300 °C and 101.3 kPa in the recirculating reactor unit (RRU). Products were sampled by syringe extraction from the recirculating stream at different contact times, and injected into a gas chromatograph equipped with flame ionization and thermal conductivity detectors. An additional GC-MS was used to confirm the identity of reaction products.

Catalytic activity and product selectivities obtained for methanol and acetaldehyde coupling reactions on $Cu_{0.5}Mg_5CeO_x$ (Figures 2,3) are summarized as follows:

a) The methanol conversion was higher than that of acetaldehyde at all contact times (Figure 2a). The methanol and acetaldehyde turnovers, based on the total number

of Cu atoms, as a function of time are shown in Figure 2b. The initial turnover rate of methanol, calculated from the slope at zero contact time, was higher than that of acetaldehyde by about a factor of 2.

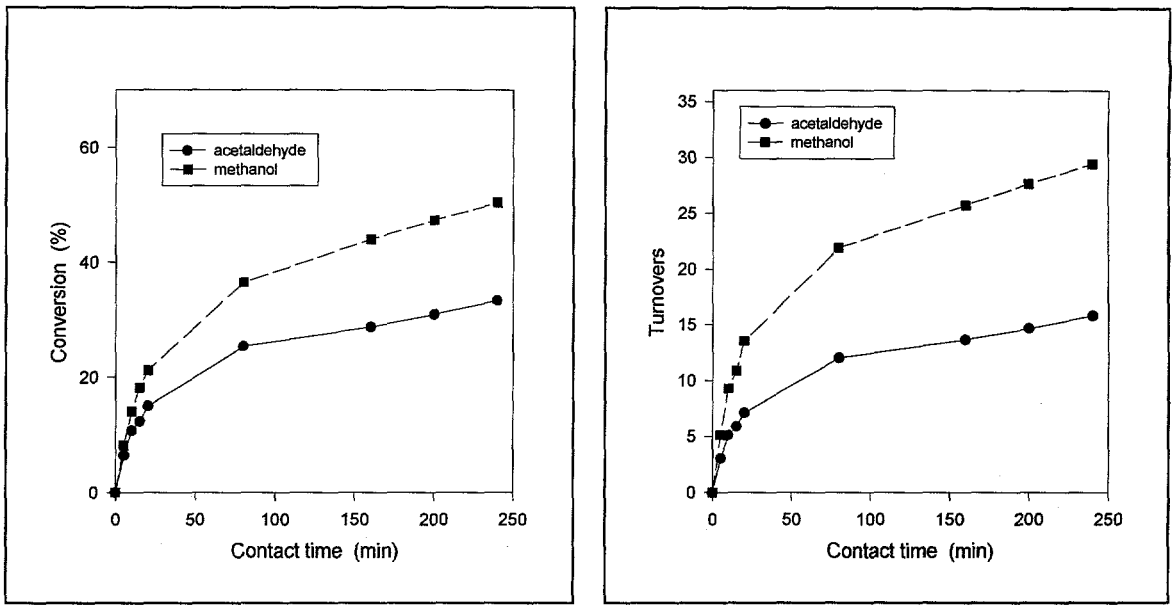

Figure 2. Methanol-acetaldehyde reactions on $Cu_{0.5}Mg_5CeO_x$ catalyst. (a) Methanol and acetaldehyde conversion as a function of contact time. (b) Methanol and acetaldehyde turnovers as a function of contact time.

b) The main product was ethanol, formed by acetaldehyde hydrogenation (Figure 3b) using the H_2 formed in methanol decarbonylation reactions. The ^{13}C-content in ethanol did not exceed its natural ^{13}C abundance, indicating that ethanol was formed exclusively from acetaldehyde at these reaction conditions.

c) Other products included CO and H_2 (from methanol decomposition), methyl acetate, propionaldehyde, isobutyraldehyde, methyl propionate and trace amounts of methyl formate (Figure 3). Analysis of the isotopic content in these products showed ^{13}C from reactant methanol. Both carbon atoms of methyl formate were labeled, indicating it formed from two molecules of methanol. Propionaldehyde contained one ^{13}C atom suggesting that it formed by the condensation of acetaldehyde with reactive formaldehyde-type intermediates formed during methanol decomposition. Isobutyraldehyde contained two ^{13}C atoms, suggesting that it formed by condensation of propionaldehyde with formaldehyde. CO_2 molecules were predominantly labeled and formed from ^{13}CO (formed by $^{13}CH_3OH$ decarbonylation) via water-gas shift reactions.

d) The remaining products showed no ^{13}C-enrichment and were formed exclusively via the self-condensation reactions of acetaldehyde and/or ethanol. These products were acetone (by acetaldehyde self-condensation), n-butyraldehyde (by acetaldehyde self-condensation), 2-pentanone (by acetaldehyde and acetone cross-condensation), ethyl acetate (by acetaldehyde-ethanol condensation), methyl ethyl ketone

(by acetaldehyde self-condensation). The reaction pathways suggested by these isotopic tracer studies are shown in Figure 3b.

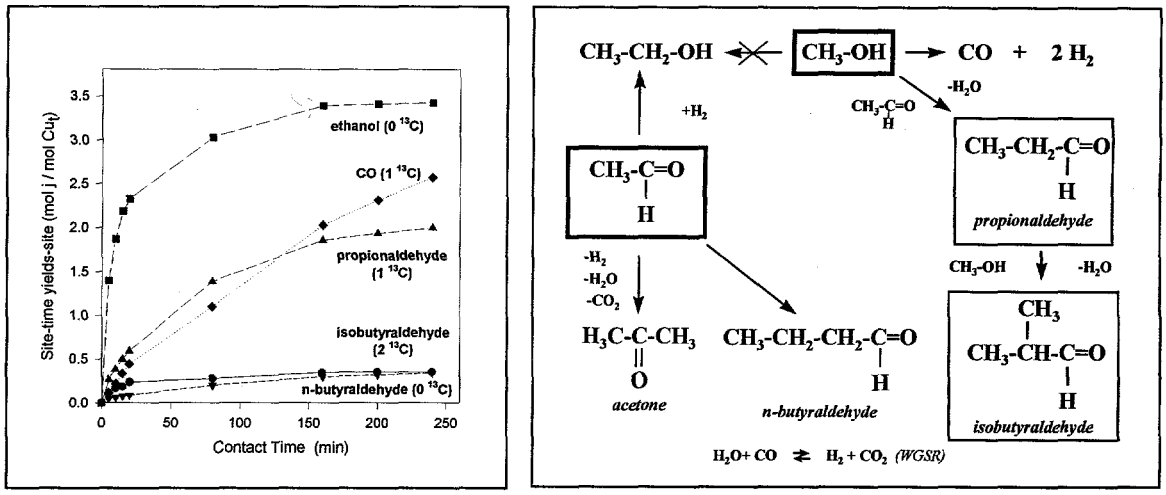

Figure 3. Methanol-acetaldehyde reactions. (a) Site yields as a function of contact time on $Cu_{0.5}Mg_5CeO_x$; (b) Reaction scheme for methanol-acetaldehyde reactions.

Cu-free Mg_5CeO_x gave a low methanol conversion of 8% (Figure 4), which is below the equilibrium conversion (90%). Also, acetaldehyde conversion was low compared to that obtained on the Cu-containing catalyst, suggesting that the predominant role of Cu is alcohol hydrogenation/dehydrogenation reactions. The Cu-free catalyst gave a 50% higher acetaldehyde conversion rate (estimated from the initial slope of the acetaldehyde curve (Figure 4)) compared to that of methanol. The basic sites on the Cu-free catalysts are responsible for acetaldehyde reactions (hydrogenation to form ethanol and self-condensation leading to higher alcohols). Yet, the dehydrogenation activity is expected to be much lower on the basic sites compared to that on Cu sites.

The unlabeled product distribution obtained on Mg_5CeO_x was similar to that on $Cu_{0.5}Mg_5CeO_x$; however, crotonaldehyde (α, β unsaturated aldehyde from acetaldehyde self-condensation) was also present in the reaction product. This unsaturated aldehyde was a final product on the Cu-free catalyst because of the low hydrogen and the lack of active Cu sites for the hydrogenation reactions leading to 1-butyraldehyde and 1-butanol.

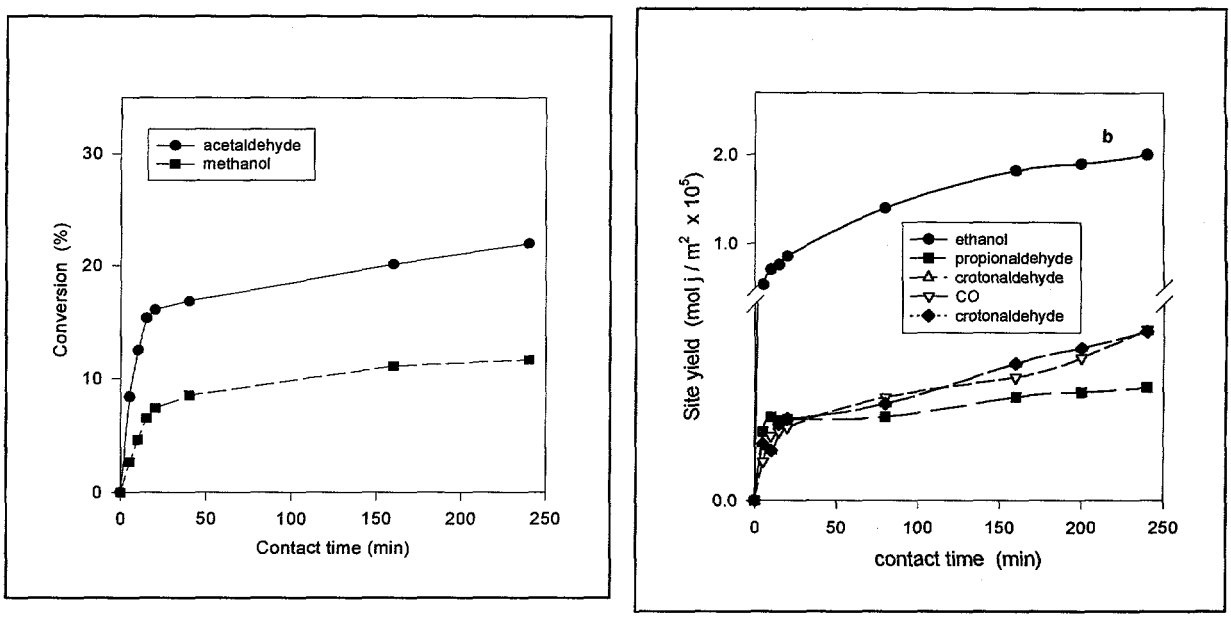

Figure 4. Methanol-acetaldehyde reactions on Mg_5CeO_x catalyst. (a) Methanol and acetaldehyde conversion as a function of contact time. (b) Site yields as a function of contact time.

The temperature-programmed surface reaction (TPSR) studies of preadsorbed ethanol showed that CO decreases the rate of base-catalyzed self-condensation reactions of ethanol to acetone, possibly due to the poisoning of basic and metal sites by the CO_2 formed from CO via water-gas shift, Boudouard reactions or oligomerization of CO on basic sites (MgO). It is believed that the highly dispersed Cu crystallites on K-$Cu_{0.5}Mg_5CeO_x$ are more likely to react with CO_2 resulting in a decrease in Cu sites. In order to address this, CO_2 effects on the catalytic activities of $CuMgCeO_x$ catalysts with different Cu loadings have been studied in ethanol coupling reactions. In a typical experiment, 3.3-4.7 kPa of CO_2 was added to a gas feed containing C_2H_5OH, H_2, CH_4 and He.

RRU07 and RRU08 were conducted on $Cu_{0.1}Mg_5O_x$ catalyst (Ce-free), with and without CO_2 in the feed, respectively. The results are summarized as follows:

a) Ethanol conversion reached an asymptotic value of ~70% in both cases (Figures 5 and 6).
b) The main product was acetaldehyde, produced by ethanol dehydrogenation.
c) The condensation products were: acetone, ethyl acetate, n-butyraldehyde, and 2-pentanone.
d) CO_2 addition decreased the rates of condensation reactions (on basic sites), but had no apparent effect on dehydrogenation (on Cu sites) (Figures 5b and 6b), suggesting that the larger Cu crystallites on $Cu_{0.1}MgO_x$ are less likely to react with CO_2 possibly because of the lack of strong metal-support interaction between Cu and ceria.

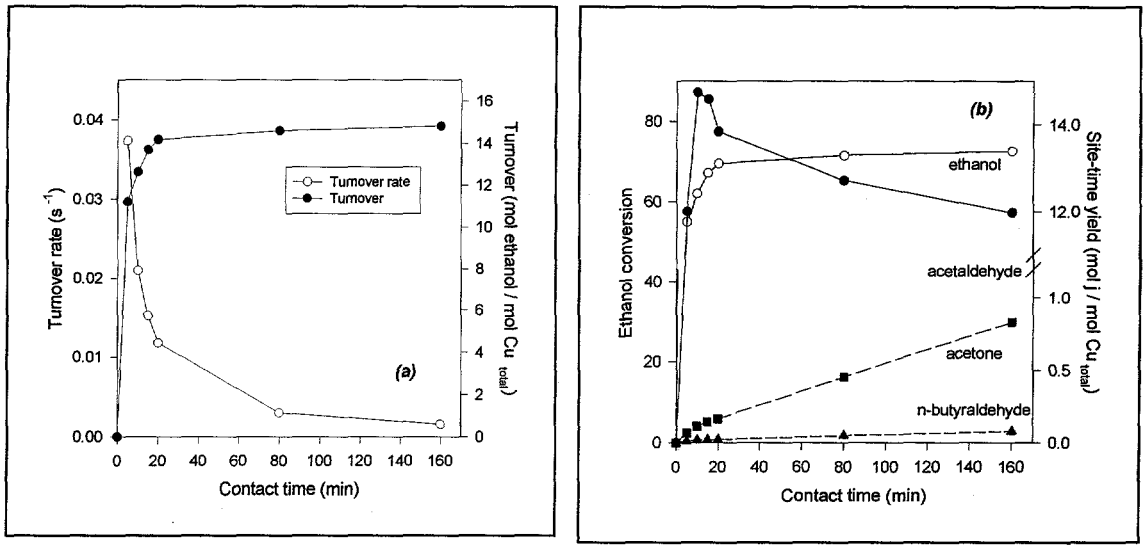

Figure 5. Ethanol reactions with CO_2-free feed gas. (a) Ethanol turnovers and turnover rates. (b) Site-time yields as a function of contact time on $Cu_{0.1}MgO_x$.

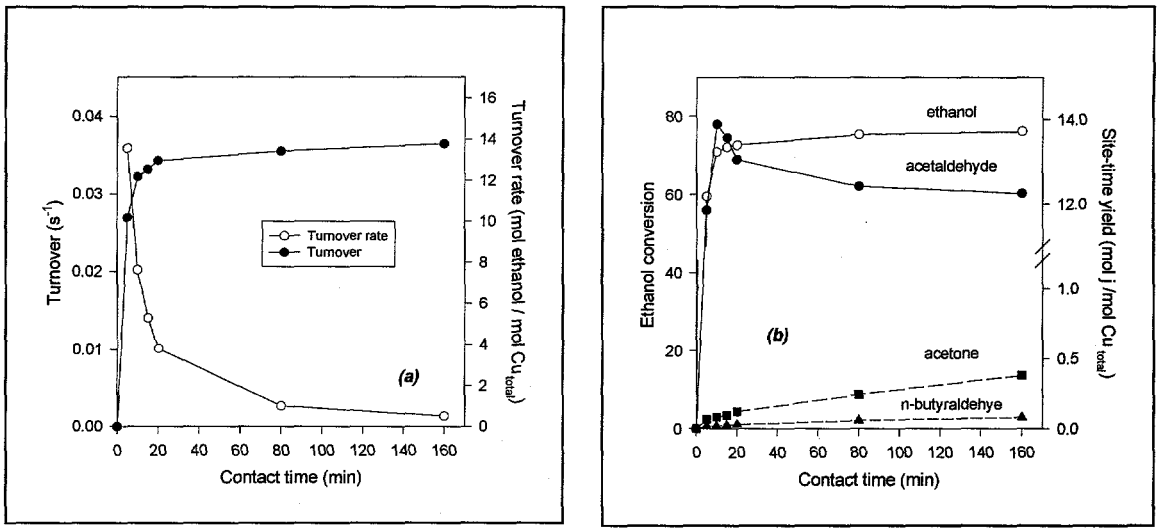

Figure 6. Ethanol reactions with CO_2-addition to feed gas. (a) Ethanol turnovers and turnover rates. (b) Site-time yields as a function of contact time on $Cu_{0.1}MgO_x$.

To address the role of Ce, RRU09 and RRU10 were conducted on K-$Cu_{0.5}Mg_5CeO_x$ catalysts with CO_2 and without CO_2, respectively. In both runs, acetaldehyde was the initial product of ethanol reactions and a reactive intermediate in the formation of acetone, n-butyraldehyde, and other oxygenates. Acetone and n-butyraldehyde were the major products. Methyl ethyl ketone, 2-pentanone and ethyl acetate were formed in trace amounts. When CO_2 was added to ethanol feeds, *both* dehydrogenation and coupling reaction rates decreased (Table 3), suggesting that both Cu

and basic sites were inhibited by CO_2. It should be pointed out that acetone production on $Cu_{0.1}MgO_x$ is much less compared to that on $Cu_{0.5}Mg_5CeO_x$, suggesting the role of ceria in promoting acetone formation. This is in agreement with the mechanism proposed in the previous quarterly report.

Table 3. Effect of CO_2 on ethanol reaction on $Cu_{0.5}Mg_5CeO_x/K$.

	Ethanol	Ethanol/CO_2
r_1	0.054	0.038
r_2	6.2×10^{-4}	2.2×10^{-4}
r_3	4.6×10^{-5}	1.0×10^{-5}

r_j are expressed in mol / mol Cu · s

The effect of CO_2 in ethanol reactions on 1 wt.% K-$Cu_{7.5}Mg_5CeO_x$ (high Cu-loading) was also investigated by adding CO_2 to ethanol feeds in order to determine the influence of Cu particle size. The results obtained in the presence and absence of CO_2 are shown in Figures 7 and 8, and summarized as follows:

a) Ethanol conversion reached an asymptotic value of ~90% in CO_2-free run and of ~75% in CO_2-added run (Figures 7 and 8).
b) The main product was acetaldehyde, produced by ethanol dehydrogenation.
c) The condensation products were: acetone, ethyl acetate, n-butyraldehyde, and 2-pentanone.
d) CO_2 addition inhibited both dehydrogenation and coupling reactions, suggesting that both Cu and basic sites were affected by CO_2 (Figures 1b and 2b).

On both Ce-containing and Ce-free $CuMgO_x$ catalysts, the basic sites required for chain-growth condensation reactions were poisoned by CO_2. CO_2 had a detrimental effect on the dehydrogenation reactions on Ce-containing $CuMgO_x$ catalysts, irrespective of Cu particle size. Owen and co-workers [11] have also reported that $CeCu_2$ materials are irreversibly deactivated by low concentrations (<1% CO_2) in H_2/CO feeds during high-pressure methanol synthesis reactions. This suggests that the strong metal-support interaction (SMSI) between Cu and Ce results in a loss of Cu sites in the presence of CO_2, possibly due to the stabilization of Cu^+ by CeO_2 via SMSI-type decoration of Cu surfaces with CeO_x.

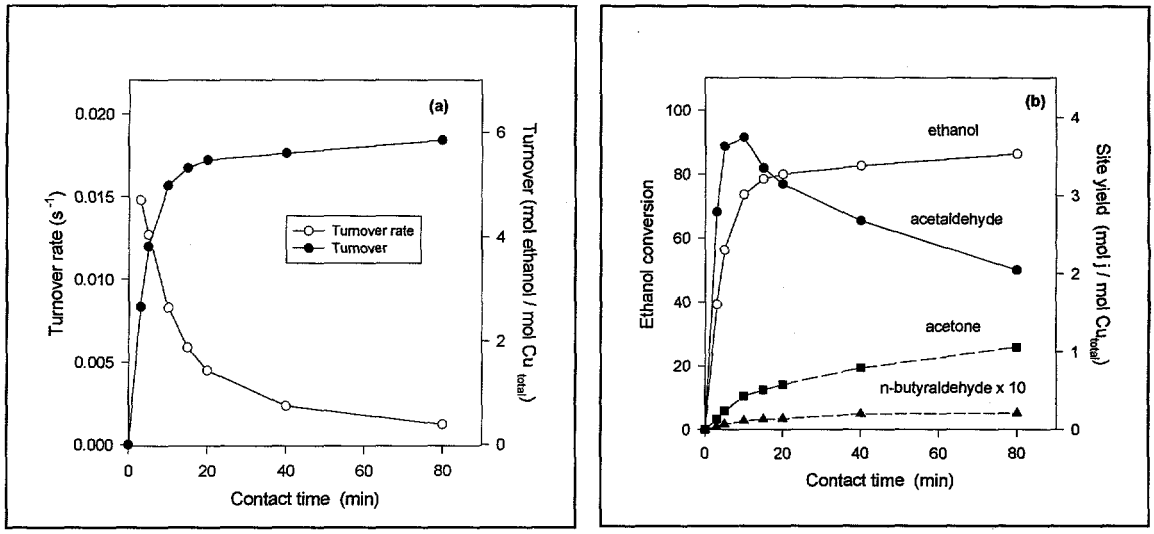

Figure 7. Ethanol reactions with CO_2-free feed gas. (a) Ethanol turnovers and turnover rates. (b) Site-time yields as a function of contact time on $Cu_{7.5}Mg_5CeO_x/K$.

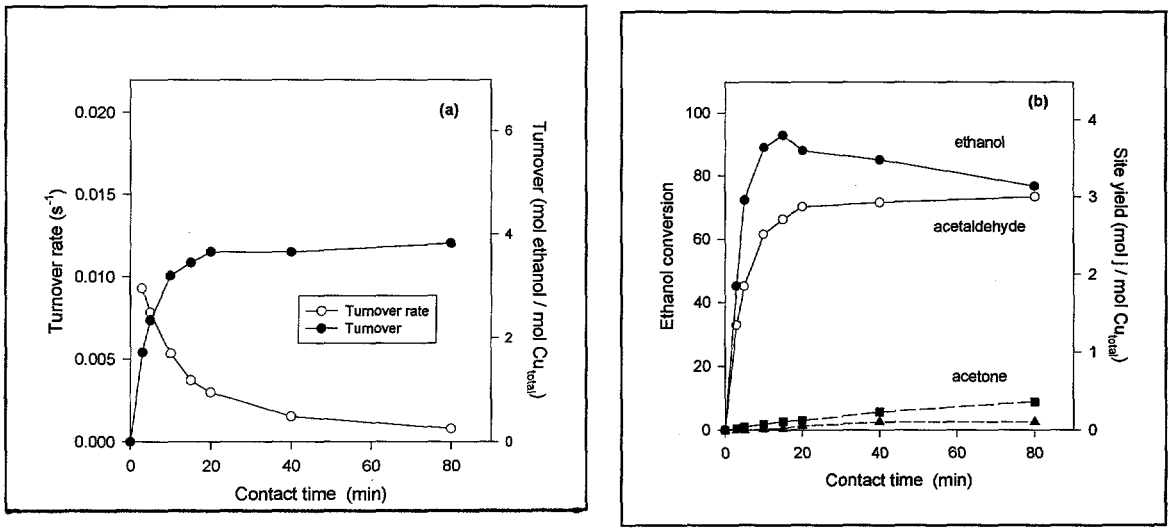

Figure 8. Ethanol reactions with CO_2-addition to feed gas. (a) Ethanol turnovers and turnover rates. (b) Site-time yields as a function of contact time on $Cu_{7.5}Mg_5CeO_x/K$.

3. Isobutanol Synthesis at High Pressure in CMRU

Space velocity studies on K-$Cu_{0.5}Mg_5CeO_x$ catalysts have shown that neither the CO conversion nor product selectivities change appreciably with space velocity [4]. These results were attributed to the progression of CO_2 inhibition of both Cu and basic sites up the length of the catalyst bed because as the space velocity was decreased, condensation reactions occurred at earlier regions in the bed, which produced CO_2 and in turn inhibited Cu and basic sites in these earlier reactor regions. Accordingly, only a small reactor region (near the inlet) continues to be active for both methanol and C_{2+}

small reactor region (near the inlet) continues to be active for both methanol and C_{2+} alcohol formation. CO_2 addition experiments were carried out on K-$Cu_{7.5}Mg_5CeO_x$ (Catalyst D) and K-$Cu_{0.5}Mg_5CeO_x$ (Catalyst E) in order to determine 1) the degree to which both Cu and basic sites are affected by CO_2, and 2) whether or not the blocking of active sites by CO_2 is reversible. Catalyst D and Catalyst E had Cu-loadings of 49 wt.% and 8 wt.%, respectively. Comparison of these catalysts in the presence of CO_2 serves to probe the differences in Cu particle size within the same class of materials. The smaller Cu particles on Catalyst E were expected to be more easily oxidized by CO_2 because of a higher degree of interaction between Cu and CeO_2 on this catalyst. Catalyst D and Catalyst E were studied at 320 °C and 4.5 MPa with an H_2/CO ratio of 1 and gas hourly space velocities (GHSV) of 1500-6000 cm^3(STP)/g-cat·h. The amount of CO_2 added to the feed on Catalyst D and Catalyst E was 3% and 1%, respectively. These CO_2 levels were chosen based on the steady-state CO_2 production before CO_2 addition.

CO_2 addition and removal on Catalyst D and Catalyst E showed similar effects on CO conversion. CO conversions were lower at all space velocities in the presence of CO_2 and removal of CO_2 from the feed resulted in a partial recovery of the CO conversion (Figures 9a,b). On both catalysts, CO_2 addition resulted in CO conversion saturation at long residence times, suggesting that these CO_2 pressures were sufficient to give shortened active beds, and thereby set upper bounds for alcohol product formation at these low CO_2 concentrations.

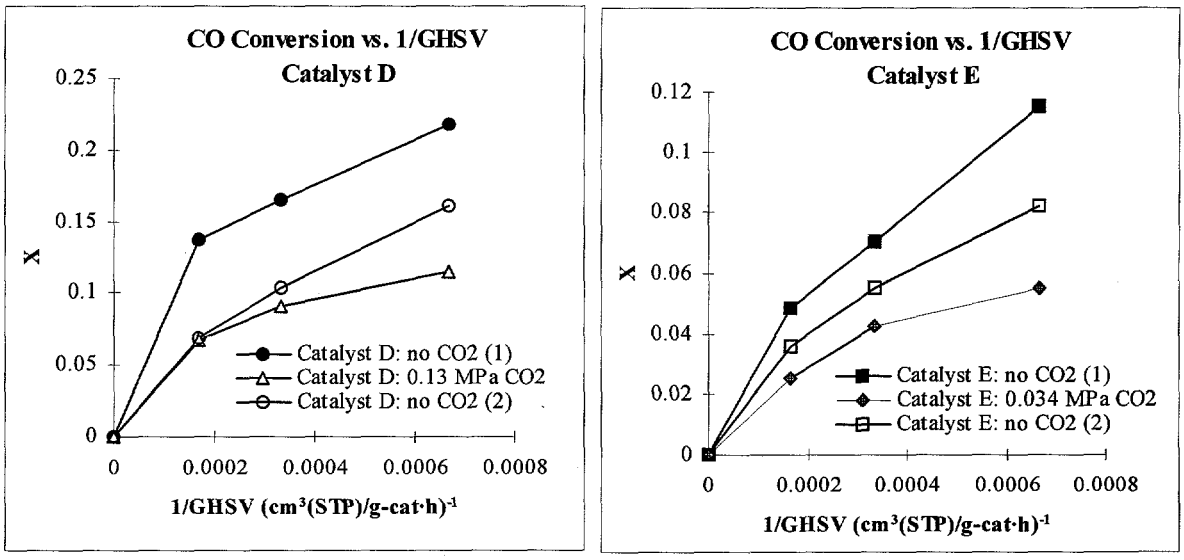

Figure 9: CO Conversion vs. Reciprocal Space Velocity. a) Catalyst D (K-$Cu_{7.5}Mg_5CeO_x$) and b) Catalyst E (K-$Cu_{0.5}Mg_5CeO_x$). T=320 °C, P=4.5 MPa.

Comparison of methanol productivities on Catalyst D and Catalyst E show that CO_2 irreversibly affected Cu sites on Catalyst D whereas inhibition effects on Cu in Catalyst E were reversible (Figure 10). Catalyst E, however, was less resistant to CO_2 oxidation, evidenced by the stronger negative dependence of methanol productivity on CO_2 pressure in the reactor (Figure 11).

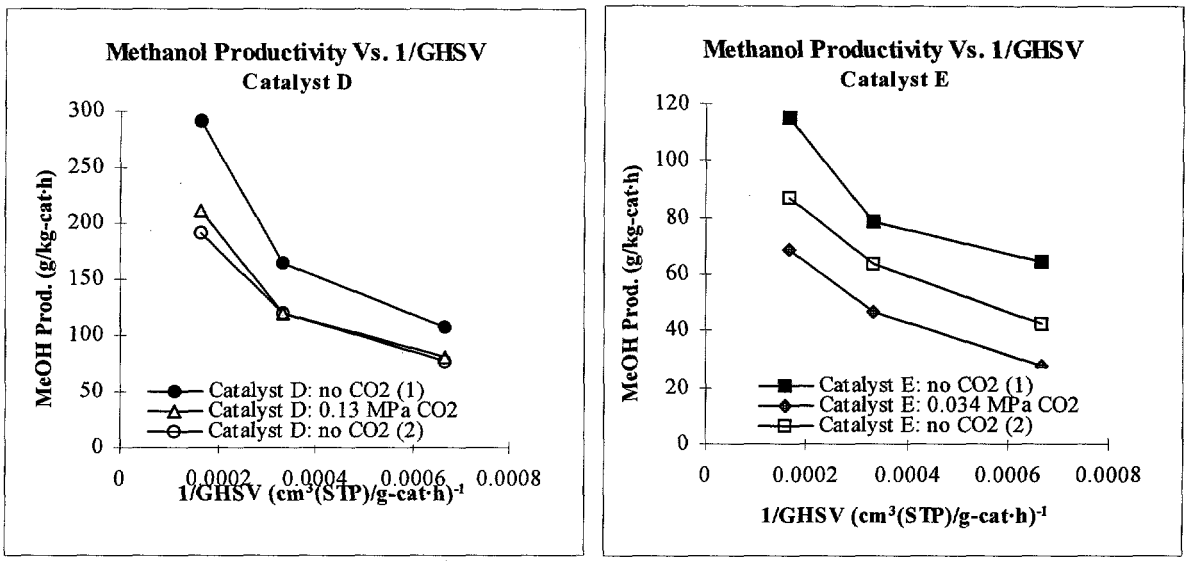

Figure 10: Methanol Productivity vs. Reciprocal Space Velocity. a) Catalyst D ($K\text{-}Cu_{7.5}Mg_5CeO_x$) and b) Catalyst E ($K\text{-}Cu_{0.5}Mg_5CeO_x$). T=320 °C, P=4.5 MPa.

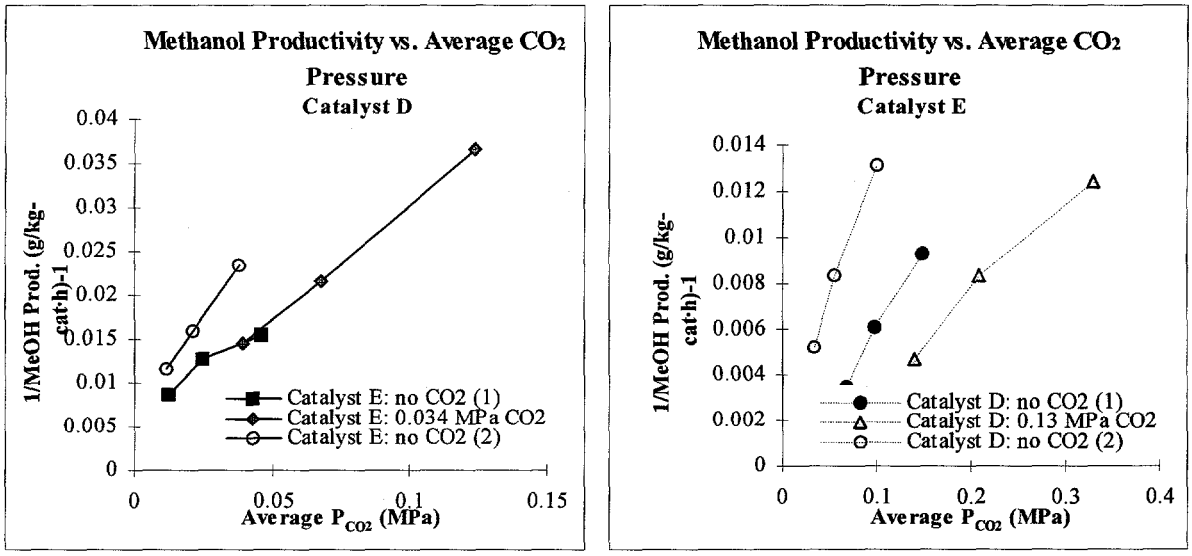

Figure 11: Methanol Productivity vs. Average CO_2 Pressure. a) Catalyst D ($K\text{-}Cu_{7.5}Mg_5CeO_x$) and b) Catalyst E ($K\text{-}Cu_{0.5}Mg_5CeO_x$). T=320 °C, P=4.5 MPa.

These observations suggest that the smaller Cu particles on Catalyst E were more easily oxidized, but were also more easily reduced upon removal of CO_2 from the feed.

The isobutanol productivity on Catalyst D decreased from 6.6 to 0.5 g/kg-cat·h at 1500 cm^3(STP)/g-cat·h with CO_2 addition while that on Catalyst E decreased from 3.7 to 0.7 g/kg-cat·h at the same space velocity (Figures 12a,b), indicating that the basic sites on Catalyst D were inhibited by CO_2 to a greater extent than those on Catalyst E. This result was attributed to the more dramatic decrease in methanol productivity on Catalyst D compared to that on Catalyst E.

The isobutanol /methanol ratio, useful for determining whether Cu or basic sites are more adversely affected by CO_2 and if CO_2 inhibition of basic sites is reversible, showed a marked decrease on Catalyst D during CO_2 addition compared with Catalyst E (Figure 13a,b). This behavior was attributed to the more dramatic decrease in methanol productivity on Catalyst D (34%) compared to Catalyst E (25%), which resulted in a smaller number of C_1^* species for condensation reactions. The isobutanol/methanol ratio on Catalyst E was recovered upon removal of CO_2 from the feed, indicating that CO_2 inhibition of basic sites on this catalyst is a reversible process (Figure 13).

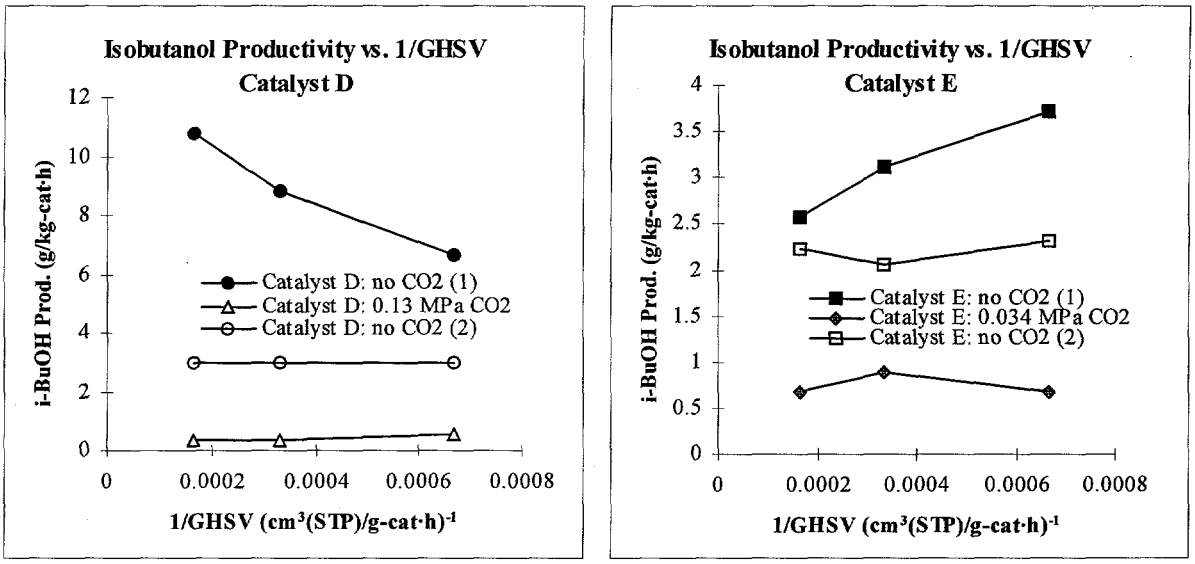

Figure 12: Isobutanol Productivity vs. Reciprocal Space Velocity. a) Catalyst D ($K\text{-}Cu_{7.5}Mg_5CeO_x$) and b) Catalyst E ($K\text{-}Cu_{0.5}Mg_5CeO_x$). T=320 °C, P=4.5 MPa.

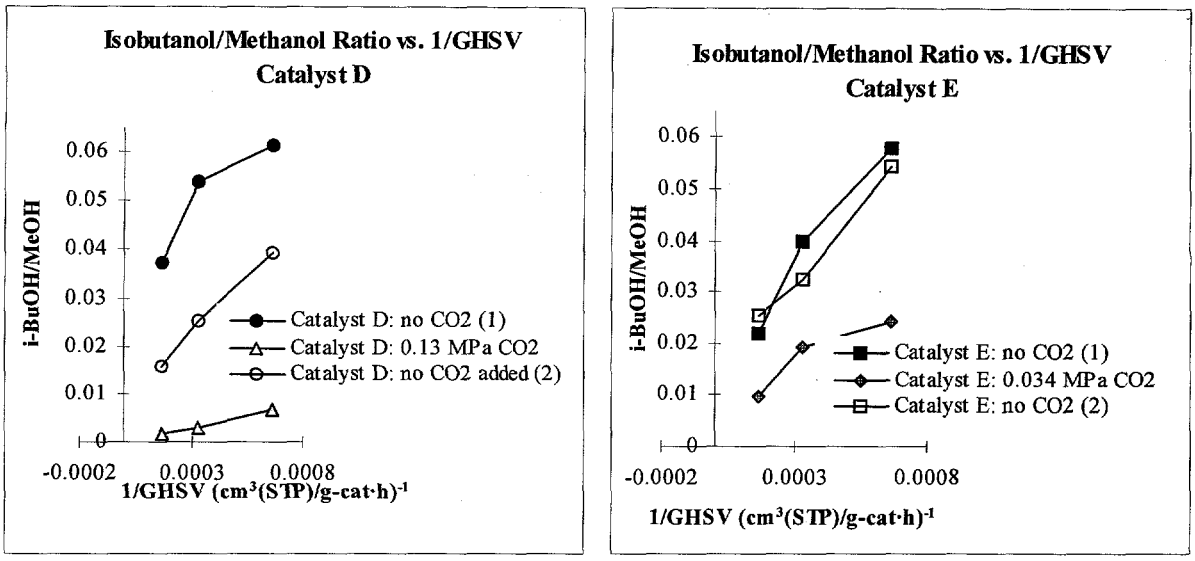

Figure 13: Isobutanol/Methanol Ratio vs. Reciprocal Space Velocity. a) Catalyst D ($K\text{-}Cu_{7.5}Mg_5CeO_x$) and b) Catalyst E ($K\text{-}Cu_{0.5}Mg_5CeO_x$). T=320 °C, P=4.5 MPa.

Space velocity studies *before* CO_2 addition were carried out on Catalyst D and Catalyst E in order to probe the true reversibility of CO_2 effects. These studies also served to probe the long-term stability of these catalysts because the two 6000 cm^3(STP)/g-cat·h data points are taken ~ 60 h apart. Catalyst E was more resistant to deactivation, by CO_2 and/or any other deactivation mechanism, than Catalyst D (Figures 14 and 15), however, both materials showed that methanol production decreased with increasing time on stream. Isobutanol formation showed slight decreases upon return to the high space velocity of 6000 cm^3(STP)/g-cat·h, a result that is attributable to the decrease in methanol production (Figures 14d and 15d). The observation that the isobutanol/methanol ratio was 100% recovered on both catalysts suggests a deactivation mechanism which affects Cu exclusively, such as Cu particle sintering or irreversible oxidation.

Results of the CO_2 addition experiments showed conclusively that the large Cu particles on Catalyst D were irreversibly affected in the presence of added CO_2. The effect of CO_2 pressure on methanol productivities for $K\text{-}Cu_{7.5}Mg_5CeO_x$ and $K\text{-}Cu_{0.5}Mg_5CeO_{7.5}$ showed that the smaller Cu particles on the latter were more easily oxidized by CO_2, but that this process was partially reversible. CO_2 inhibition of basic sites on $K\text{-}Cu/MgO/CeO_2$ catalysts is reversible. Finally, the space velocity studies before CO_2 addition, conducted at 6000, 3000, 1500, and 6000 cm^3(STP)/g-cat·h in that order, showed that the $K\text{-}Cu/MgO/CeO_2$ catalysts suffer a deactivation process that affects Cu exclusively. The apparent deactivation might be explained by Cu particle sintering or irreversible oxidation.

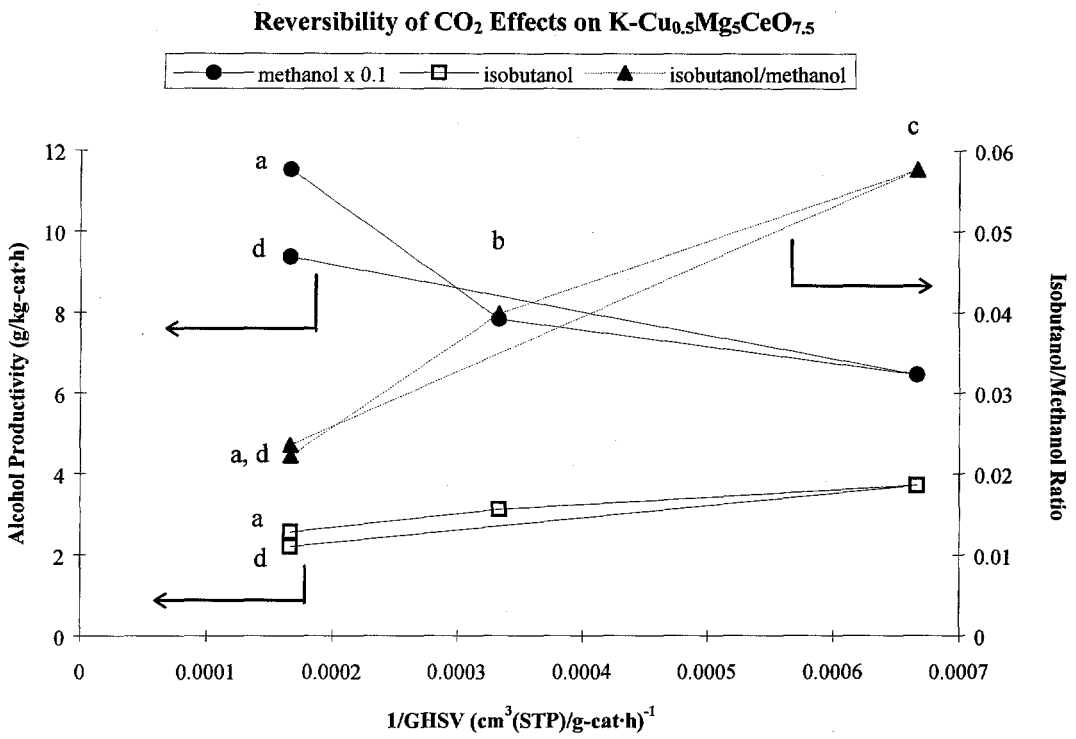

Figure 14: Methanol and Isobutanol Productivities and Isobutanol/Methanol Ratio vs. Reciprocal Space Velocity. Catalyst E at 320 °C, 4.5 MPa. a) 6000 b) 3000 c) 1500 d) 6000 cm^3(STP)/g-cat·h.

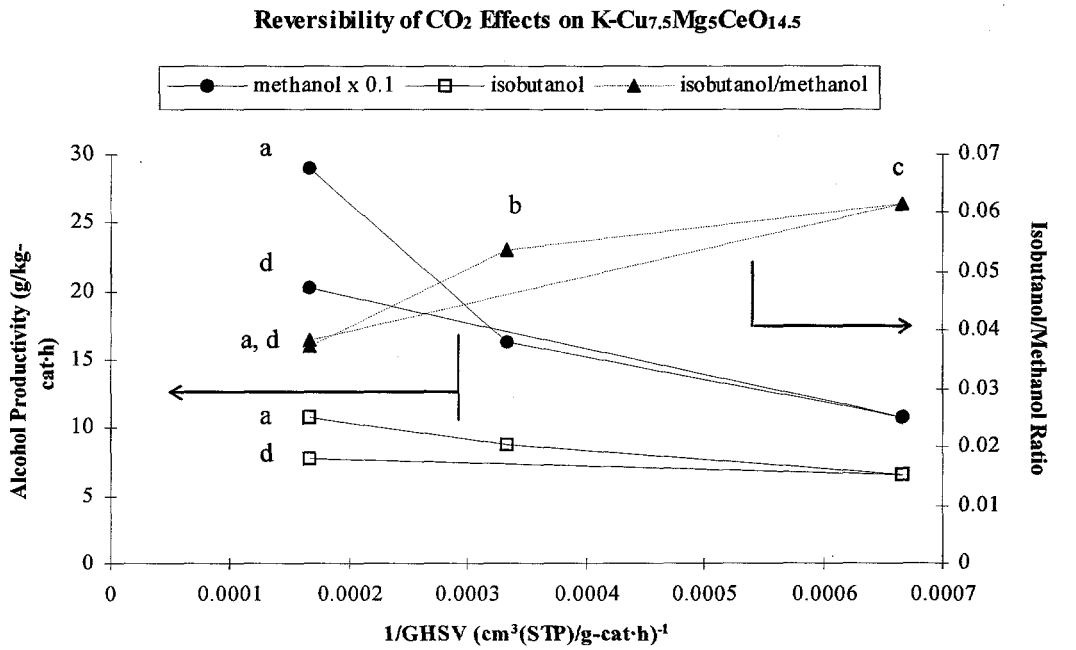

Figure 15: Methanol and Isobutanol Productivities and Isobutanol/Methanol Ratio vs. Space Velocity. Catalyst D at 320 °C, 4.5 MPa. a) 6000 b) 3000 c) 1500 d) 6000 cm^3(STP)/g-cat·h.

1-Propanol Addition to H_2/CO Feeds on K-$Cu_{7.5}Mg_5CeO_x$

1-Propanol was added to H_2/CO feeds on Catalyst D to probe C_{3+} growth pathways on K-Cu/Mg/CeO_2 catalysts. The experiment was carried out at 320 °C and 4.3 MPa with $H_2/CO/Ar$/1-propanol= 44.8/44.8/9.9/0.5. This experiment was performed after the CO_2 addition study, approximately 200 h into the run. Catalytic activity was first obtained without 1-propanol addition at 593 K and 4.3 MPa with a H_2/CO ratio of 1. The reactor was then purged in H_2 at 593 K and atmospheric pressure for 1 h before analyzing the 1-propanol-containing feed (reactor bypassed in stagnant H_2 at 593K and atmospheric pressure). The amount of 1-propanol added was approximately 30% of the methanol produced in the 1-propanol addition experiment.

		1-Propanol addition
	CMRU-21C	**CMRU-21D**
T (K)	593	593
P (MPa)	4.5	4.3
GHSV (cm^3(STP)/g.cat·h)	1500	1500
H_2/CO feed ratio	1	1
CO Conversion	16.0%	15.4%
Rate (mmol COconverted/g-cat·h)	4.31	4.25
Product Selectivitities[a] (mol% C)		
methanol	**60.56**	**53.25**
ethanol	2.81	1.18
1-propanol	4.31	4.28
isopropanol	3.01	1.26
2-butanol	0.39	0.71
isobutanol	**4.12**	**14.91**
1-butanol	0.17	1.46
1-pentanol	0.06	0.94
2-methyl-1-butanol	0.54	1.25
1-hexanol	0.15	0.39
2-methyl-1-pentanol	0.21	1.24
CH_4	9.48	8.60
C_{2+} paraffins	2.28	2.83
CO_2	29.81	34.75

Table 4: Product selectivities on Catalyst D. a) without propanol addition, b) with propanol addition (Feed $H_2/CO/Ar/PrOH$ = 44.8/44.8/9.9/0.5). [a]Selectivities are normalized on a CO_2-free basis (except CO_2).

Table 4 shows that 1-propanol addition decreased the CO conversion only slightly, from 16.0% to 15.4%, and resulted in increased alcohol selectivities for isobutanol, 1-butanol, 1-pentanol, 2-methyl-1-butanol, and 2-methyl-1-pentanol. The significant increase in isobutanol selectivity suggests that isobutanol forms by the condensation of methanol (formaldehyde) and 1-propanol (propionaldehyde). Comparison of the isobutanol/1-propanol ratio (3.48) and the 1-butanol/1-propanol ratio

(0.34) during 1-propanol addition shows that growth via β-branching was much more favorable than linear growth on K-Cu/Mg/CeO_2. Isobutanol is a kinetic endpoint before and during 1-propanol addition because it has only one α-hydrogen available for abstraction, and this α-hydrogen is sterically hindered.

Increased selectivities to 2-methyl-1-butanol and 2-methyl-1-pentanol during 1-propanol addition are the result of the increased selectivities to 1-butanol and 1-pentanol, respectively. 2-methyl-C_n alcohols form by the condensation (β–branching) of C_1 with C_n surface aldehydes.

Task 4: Identification of Reaction Intermediates

During this reporting period, the construction of a high-pressure and high-temperature IR cell has been completed (Figure 16). It consists of a 25.4-mm i.d. stainless-steel tube with gas inlet, outlet, thermocouple port and cooling water or air lines. CaF_2 window was used because of its IR transmittance ability in the range of 1000 - 3500 cm^{-1} and because of its stability at temperatures up to 500 °C. The sample holder, made of stainless steel, has three notches for thermocouple, gas inlet and oulet. Two CaF_2 rods were placed on both sides of the sample holder inside the reactor in order to reduce void volume. The smaller void volume could minimize gas-phase IR, which will become important in the study of high-pressure syngas-to-alcohol reactions. The cell is resistively heated externally with an OMEGALUX mineral insulated heating cable.

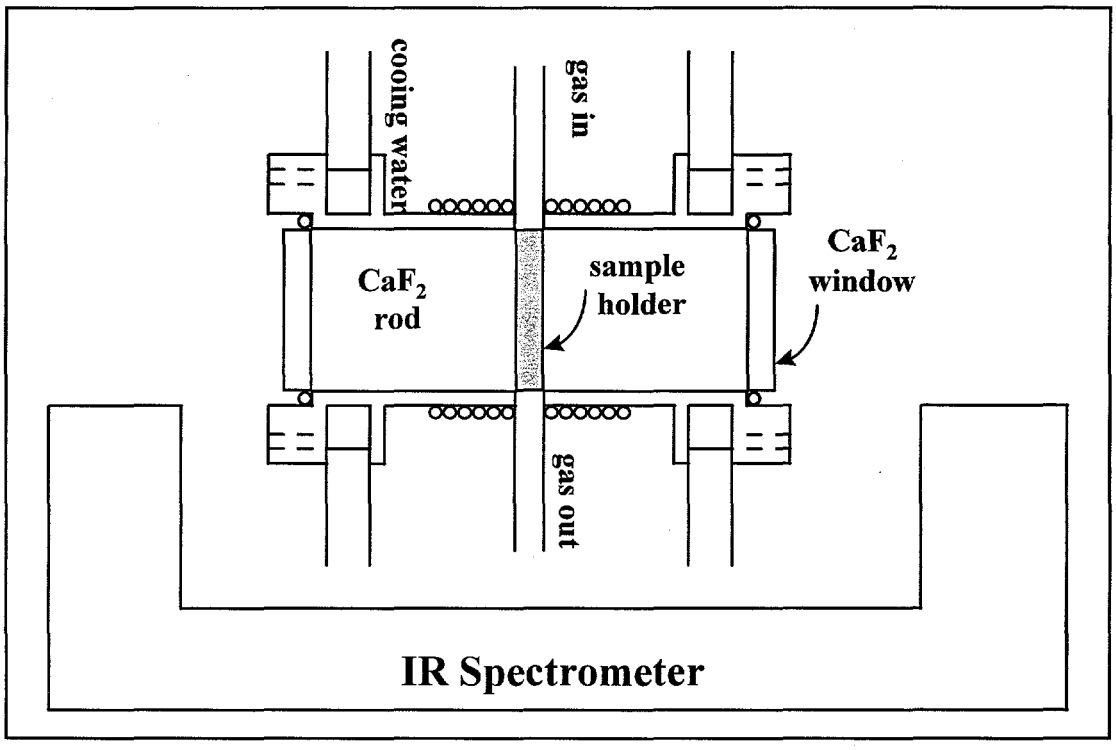

Figure 16. High-pressure and high-temperature in-situ IR cell/reactor

4.1. Determination of Basic Site Density and Strength

Because of the role of basic sites in the chain-growth reactions leading to isobutanol, it is important to determine the basic site density on the working catalyst. In this study, the density of basic sites was determined using a $^{13}CO_2/^{12}CO_2$ exchange method. This method provides a direct measure of the number of basic sites *"kinetically available" for adsorption and catalytic reactions at reaction conditions.* In addition, this technique gives the distribution of reactivity for such basic sites. In this method, a pre-reduced catalyst was exposed to a 0.1 % $^{13}CO_2$/He stream and after $^{13}CO_2$ reached a constant level in the effluent, the flow was switched to 0.1 % $^{12}CO_2$/He. The relaxation of the $^{13}CO_2$ removed from the surface was followed by mass spectrometry. The exchange capacity (Table 5) and dynamics (Figure 17) at reaction temperature were calculated from these data.

Table 5. Composition, surface area, basic site density of mixed metal oxides

[a]Sample	[b]Sg, m^2/g	[b]Cu, dispersion, %	Exchangeable CO_2 at 300 °C 10^{-6} mol/m^2	CO_2 desorbed during TPD at T < 300 °C 10^{-6} mol/m^2
1.2 wt% K-$Cu_{7.5}Mg_5CeO_x$	92	5	3.28	0.91
5.3 wt% K-Mg_5CeO_x	53	/	----	----
0.1 wt% K-$Cu_{0.5}Mg_5CeO_x$	167	23	1.20	0.62
1.1 wt% K-$Cu_{0.5}Mg_5CeO_x$	147	14	2.33	0.64
2.6 wt% K-$Cu_{0.5}Mg_5CeO_x$	93	7	3.48	0.43

[a] Bulk composition measured by atomic absorption.
[b] Total surface area determined by N_2 BET adsorption at 77 K.
[c] Dispersion calculated from the ratio of surface Cu (determined by N_2O decomposition at 90 °C [7,8]) to the total number of Cu atoms in the catalyst.

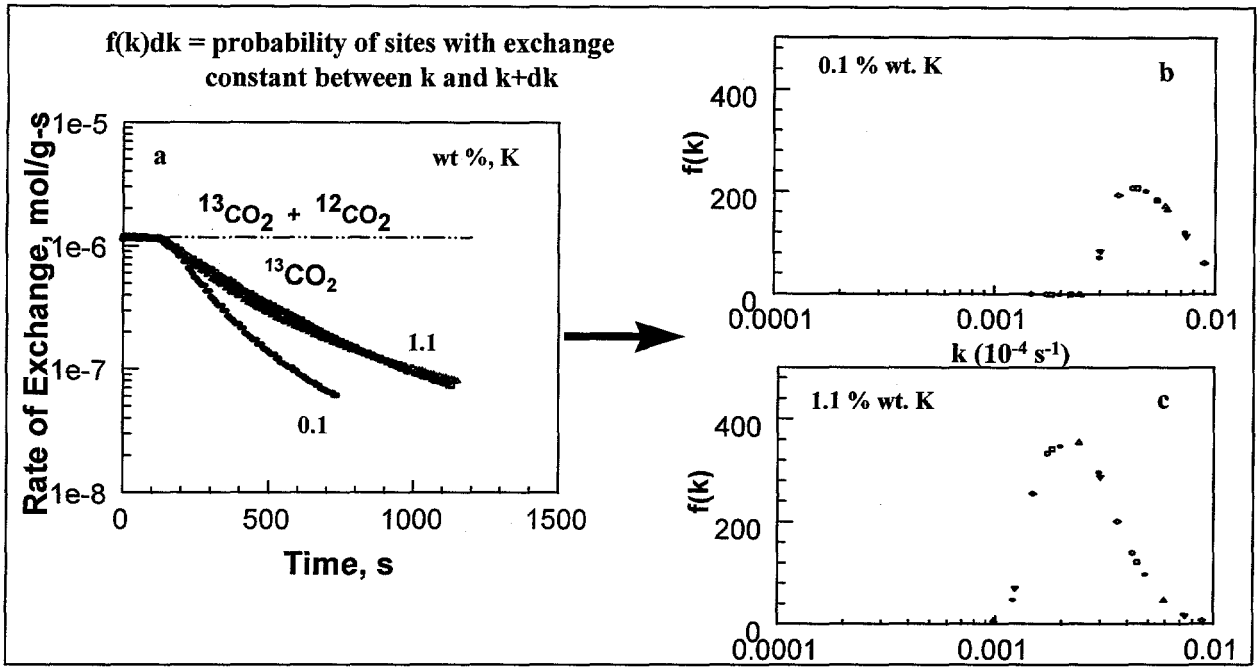

Figure 17. Exchange methods probe dynamics on non-uniform surface of K-$Cu_{0.5}Mg_5CeO_x$.

The response curves obtained by $^{13}CO_2/^{12}CO_2$ switch experiments on K-promoted $Cu_{0.5}Mg_5CeO_x$ are shown in Figure 17a. The exchange capacity is determined from the area of the $^{13}CO_2$ curve and is reported in Table 5. The local slope in this semi-logarithmic plot reflects exchange dynamics and thus the kinetic behavior of basic sites. The curvature of the semi-logarithmic curve indicates the heterogeneity of surface basic sites since a linear line would be expected of a uniform surface. Short relaxation times (e.g. 0.1 wt % K) reflect short CO_2 surface lifetimes, high exchange rates, and more weaker basic sites. K increases not only the basic site density in $Cu_{0.5}Mg_5CeO_x$ (Table 5) but also the strength of basic sites, as shown by the shift in site distribution to lower exchange rate constants (Figures 17b, 17c). The distribution of exchange rate constants (Figures 17b and 17c) were obtained using inverse Laplace transform deconvolution methods [12]. In contrast with CO_2 temperature-programmed desorption (TPD), $^{13}CO_2/^{12}CO_2$ exchange methods probe the density and reactivity of basic sites at reaction temperatures, without contributions from unreactive carbonates and without disrupting the steady-state surface composition of the catalytic solid. The competitive adsorption of CO_2 with aldol-coupling precursors on basic sites appears to be one of the hurdles in achieving high isobutanol synthesis rates at low temperatures.

The basic site densities determined by the conventional temperature-programmed desorption (TPD) of CO_2 are also listed in Table 5. In the TPD experiment, CO_2 is adsorbed on the pre-reduced catalyst at room temperature. The catalyst surface is subsequently flushed with He to remove gas phase and weakly adsorbed CO_2 before linearly ramping the temperature, and measuring the desorption profile of CO_2 by mass spectrometry (Figure 18). This method gives both physically and chemically adsorbed

CO_2. Nevertheless, the number of basic sites determined from CO_2 TPD based on the total amount of CO_2 desorbed below 300 °C is significantly lower than that measured by the $^{13}CO_2/^{12}CO_2$ switch experiment.

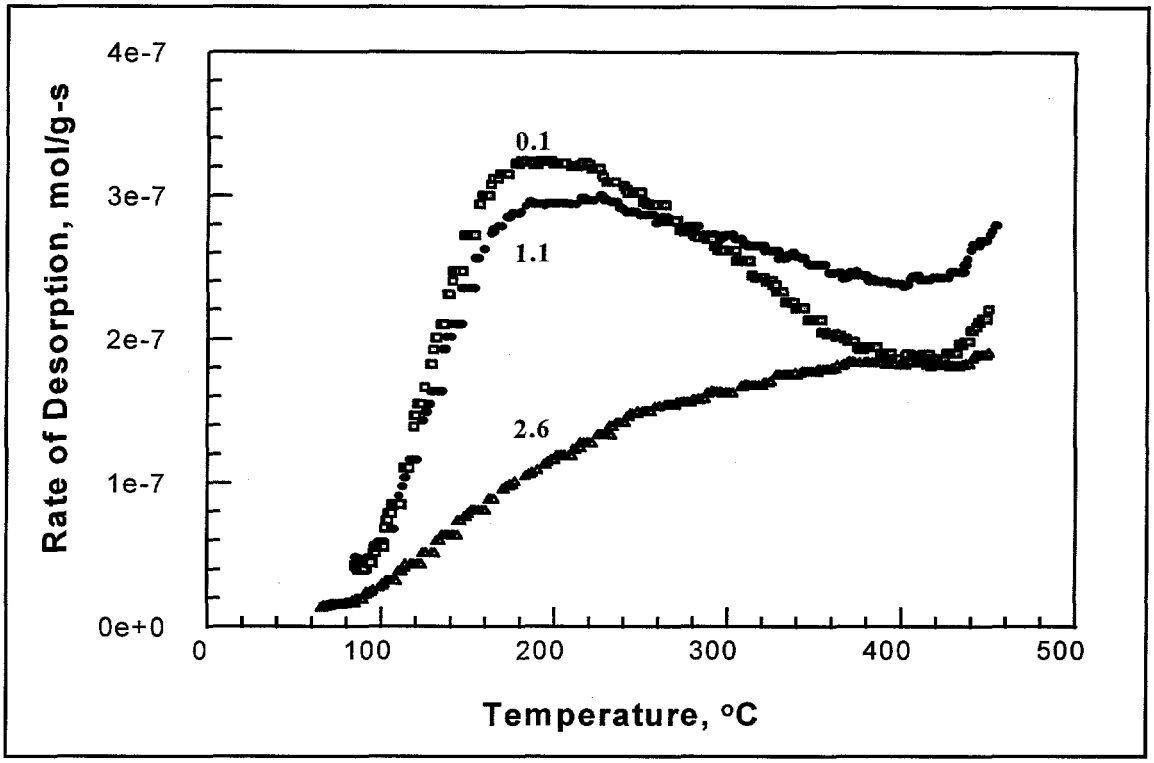

Figure 18. CO_2 temperature-programmed desorption spectra in He on K-$Cu_{0.5}Mg_5CeO_x$

4.2. *In-situ IR Studies on Surface Intermediate Species during Ethanol Surface Reactions*

The temperature-programmed surface reactions of ethanol on $Cu_{0.5}Mg_5CeO_x$ catalysts reveal the formation of acetone and crotonaldehyde. Surface acetate species are believed to be the precursor to acetone. By monitoring surface species and the change in the intensity of their vibrational IR bands with respect to temperatures using in-situ IR, it is possible to address the role of each individual surface species in chain-growth reactions. Ethanol and d_6-ethanol reactions on $Cu_{0.5}Mg_5CeO_x$ and its component oxides (MgO, CeO_2, Mg_5CeO_x and $Cu_{0.5}Mg_5CeO_x$) are being carried out, and the results obtained on MgO at different temperatures are shown in Figure 19.

The sample disk (10 mg/cm^2) was pretreated at 450 °C in flowing He for 30 min followed by H_2 treatment at 350 °C for another 30 min. The temperature was raised to 400 °C upon H_2 removal in order to obtain the background spectra. The disk was cooled to room temperature in stepwise manner for recording background spectra from 400 °C at intervals of 100 °C. The adsorbate (ethanol) vapor was introduced into the IR cell at room temperature (25 °C). After adsorption for 10 min, physically adsorbed and gas phase ethanol were removed by He purging at the same temperature. Decomposition of

the adsorbed species was investigated at elevated temperatures in a stepwise manner from 25 °C to 400 °C and *in-situ* IR spectra were taken 5 min after the desired temperature was achieved.

Figure 19a shows the spectrum recorded after purging the sample with helium at 25 °C for 30 min. Bands observed in the frequency region 3000-2800 cm^{-1} are attributed to (CH_3) and (CH_2) of adsorbed ethanol and ethoxide species, respectively. The bands near 1100 cm^{-1} are due to C-O of surface ethoxide species. The three distinct bands at 1060, 1108 and 1144 cm^{-1} suggest that three types species are formed by adsorption of ethanol at room temperature (13,14). At 200 °C, the band at 1108 cm^{-1} disappeared, and the other two bands were weakened. The former might be due to the weakly bonded ethoxide or undissociated adsorbed ethanol species. The deformation modes of methyl and methylene groups are characterized by the bands in the region of 1300-1500 cm^{-1}. The broad band centered at 3600 cm^{-1} shows the formation of surface OH groups from the dissociative adsorption of ethanol. At 100 °C (Figure 19b), all the bands decrease owing to the desorption of surface ethoxide in the form of C_2H_5OH. Interestingly, the ratio of the intensity of the band near 3730 cm^{-1} to that of the broad band centered around 3600 cm^{-1} increased with increasing temperature (Figures 19a-c), suggesting that the dehydroxylation of MgO leads to isolated hydroxyl species.

Both the band at 1380 cm^{-1} and the ones at 2800-3000 cm^{-1} decreased with increasing temperatures (Figures 19a-c), and disappeared at 300 °C, which again indicates that these bands arise from (CH_3) and (CH_2) species. The decrease in the ratio of 2925 cm^{-1} band to 2967 cm^{-1} band (Figures 19a-c) indicates the disappearance of methylene species at a faster rate compared to that of methyl group. This may be attributed to the dehydrogenation of ethoxide species on MgO surface as illustrated by the following reaction:

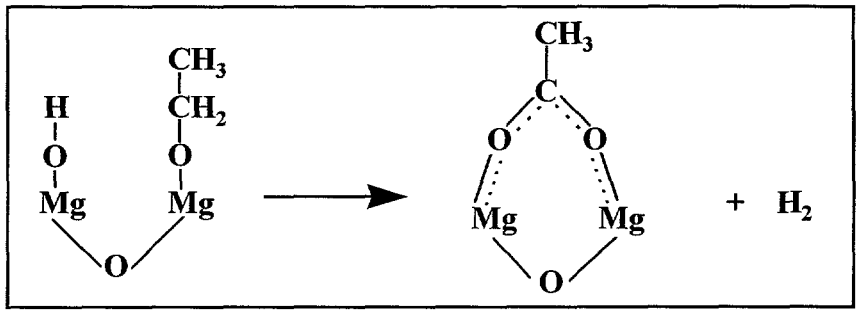

Similar mechanism has been proposed on the oxidation of surface methoxide species on MgO (15). The evolution of H_2 has been confirmed by temperature-programmed surface reactions of ethanol on MgO. As temperature increased to 300 °C, C-C cleavage occurred, resulting in the disappearance of C-H bands (2800-3000 cm^{-1}) and leaving the carbonate species on MgO surface (Figures 19d, e).

Task 5: Bench Scale Testing at Air Products and Chemicals

No activities were performed during this reporting period.

REFERENCES:

1. C.R. Apesteguia, S.L. Soled, S. Miseo, U.S. Patent No. 5,387,570. Issued Feb. 7, 1995 to Exxon Research & Engineering Co., Florham Pk., N.J.
2. D.J. Driscoll, W. Martir, J.-X. Wang, and J. H. Lunsford, *J. Am. Chem. Soc.*, **107,** 58-63 (1985).
3. J.H. Lunsford, M.D. Cisneros, P.G. Hinson, Y. Tong, and H. Zhang, *Faraday Discuss. Chem. Soc.*, **87**, 1-10 (1989).
4. A. Zecchina, S. Coluccia, G. Spoto, D. Scarano, and L. Marchese, *J. Chem. Soc., Faraday Trans.*, **86(4),** 703-709 (1989).
5. M. Xu, B.L. Stephens, M. Gines, and Iglesia, E., 13th Pittsburgh Coal Conference, September 3-7, 1996.
6. J.C. Slaa, J.G. van Ommmen, and J.R.H. Ross, *Catal. Today* **15** (1992) 129.
7. A. Sofianos, *Catal. Today* **15** (1992) 149.
8. G.A. Vedage, P.B. Himelfarb, G.W. Simmons, and K. Klier, *ACS Symp. Ser.* **279** (1985) 295.
9. D.J. Elliot, and F. Penella, *J. Catal.* **119** (1989) 359.
10. M. Xu, B.L. Stephens, M.J.L. Gines, T. Wang, and I. Iglesia, *Quarterly Report to DOE*, January 1-March 31 1996.
11. R.M. Nix, R.W. Judd, R.M. Lambert, J.R. Jennings, and G. Owen, *J. Catal.*, **118**, 175- 191 (1989).
12. M. DePontes, G.H. Yokomizo and A.T. Bell, J. Catal. 104 (1987) 147-155.
13. C. Li, K. Domen, K. Maruya, and T. Onishi *J. Catal.* **125**, 445-455 (1990)
14. V.A. Ivanov, J. Bachelier, F. Audry and J.C. Lavalley *J. Molec. Catal.* **91**, 45-59 (1994)
15. R.O. Kagel, and R.G. Greenler *J. Chem. Phys.* **49**, 1638-47 (1967)

4. PARTICIPATING PROJECT PERSONNEL

Mingting Xu
Postdoctoral Fellow

Marcelo J. L. Gines
Postdoctoral Fellow

Brandy L. Stephens
Graduate Student

James Elliot
Undergraduate Researcher

Bernard A. Toseland
Sub-Contractor
Air Products and Chemicals

Enrique Iglesia
Principal Investigator

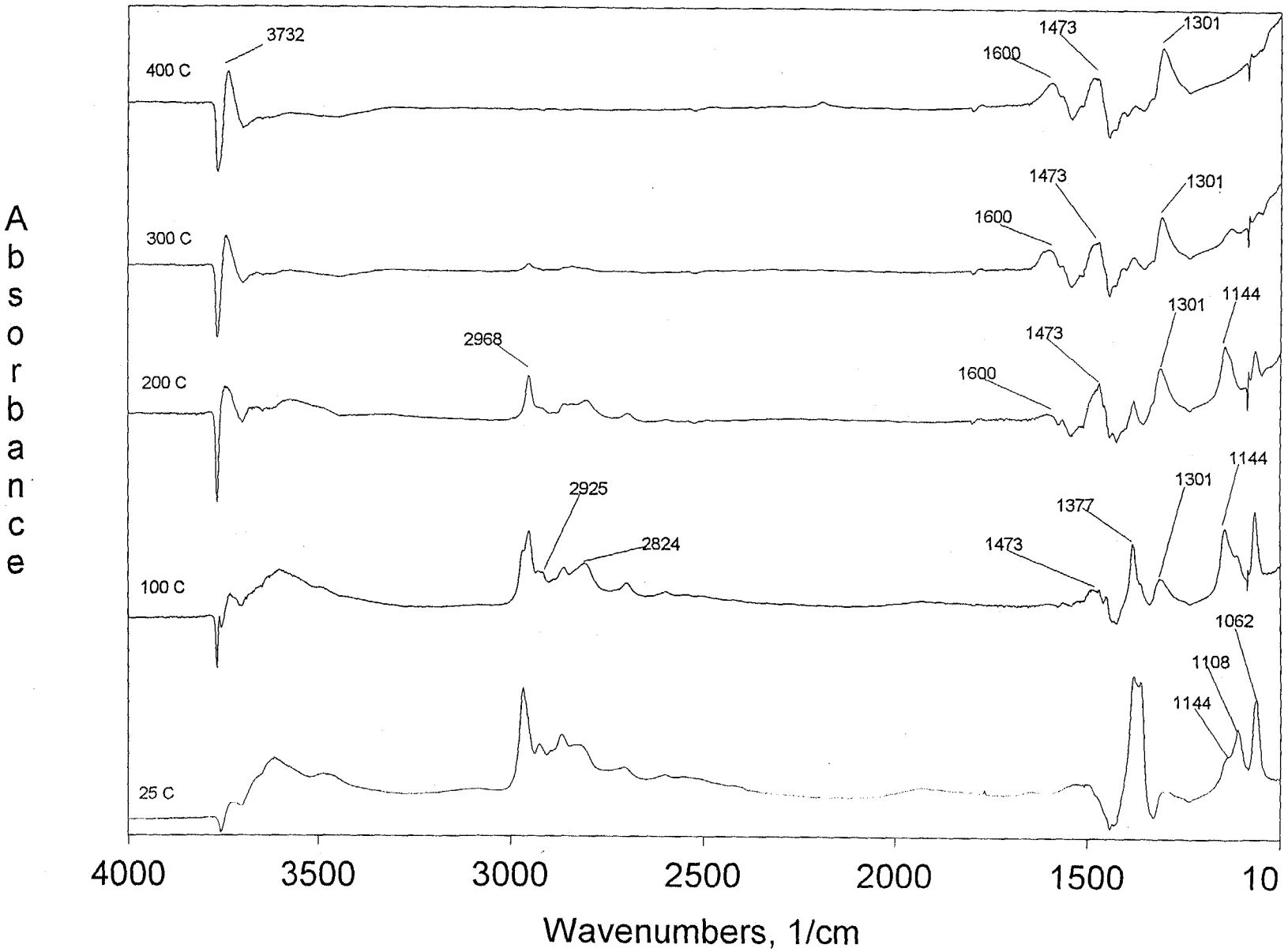

Figure 19. IR spectra of adsorbed ethanol on MgO

DOE F 1332.3
(11-84)

U.S. DEPARTMENT OF ENERGY
MILESTONE SCHEDULE ☐ PLAN ☒ REPORT

FORM APPROVED
OMB 1901-1400

1. TITLE	2. REPORTING PERIOD	3. IDENTIFICATION NUMBER
ISOBUTANOL METHANOL MIXTURE FROM SYNGAS	April 1, 1996 - June 30, 1996	DE - AC22 - PC94PC066

4. PARTICIPANT NAME AND ADDRESS	5. START DATE	6. COMPLETION DATE
Department of Chemical Engineering University of California - Berkeley	Oct 1994	Sept 1997

7. ELEMENT CODE	8. REPORTING ELEMENT	9. DURATION	10. PERCENT COMPLETE a Plan	b Actual
	Task 3	Complete design, construction and start-up of packed bed reactor module	100	100
	Task 2	Prepare Cu-based catalyst compositions and characterize structure, surface area, and effectiveness of several synthetic approaches	100	100
	Task 2	Choose four promising materials for catalyst evaluation	100	100
	Task 3	Construct recirculating reactor module Establish reaction pathways and rate-determining steps	100	100
	Tasks 2 & 3	Identify catalyst components necessary to catalyze rate-determing steps that have been determined	100	100
	Tasks 2 & 3	Identify synthetic techniques to increase the reactivity and accessibility of such required sites	100	100
	Task 4	Complete construction and start-up of temperature programmed surface reaction apparatus and design of high-pressure infrared cell	100	100
	Task 4	Design and construction of high-pressure infrared cell	100	100
	Task 4	Calibrate between UCB and APCI laboratories by testing two selected catalysts in slurry reactors	100	20
	Task 2	Determine the density and reactivity of the required sites and implement synthetic methods to improve them	40	40

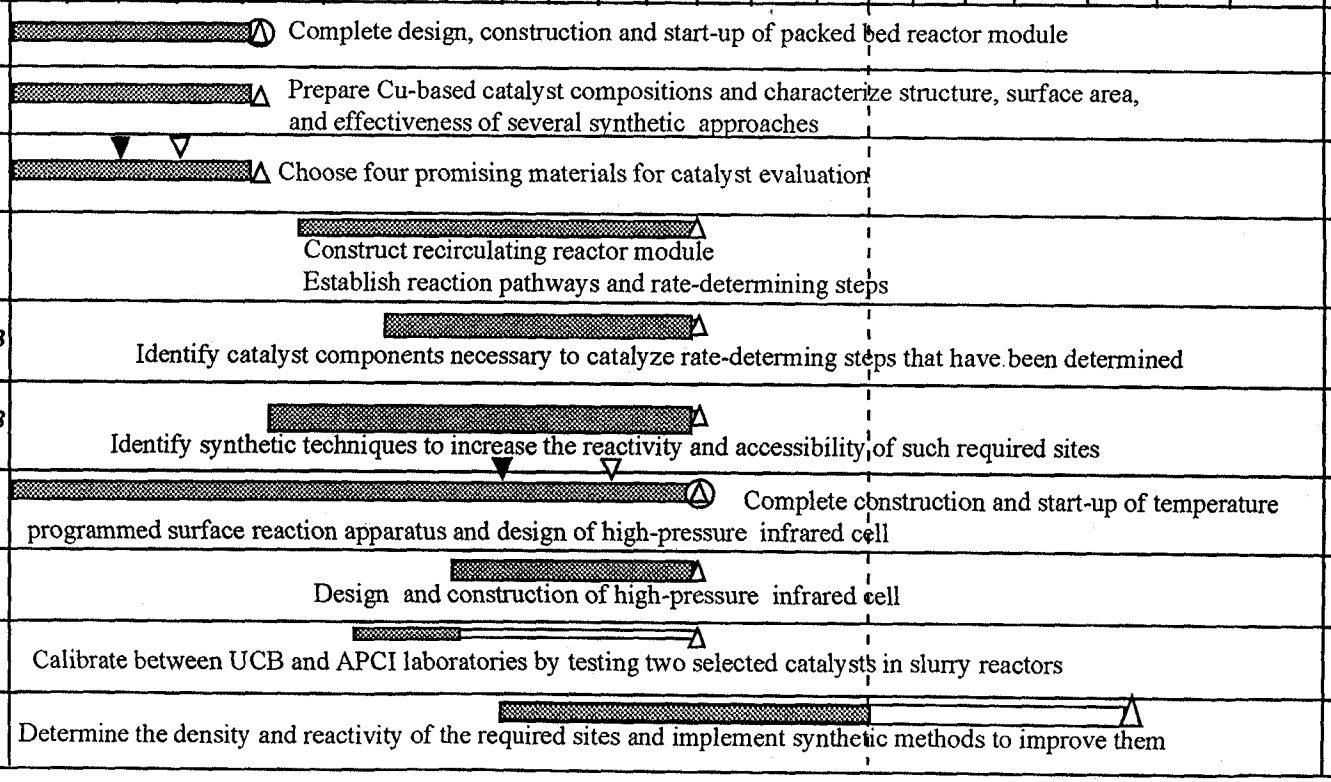

DOE F 1332.3
(11-84)

U.S. DEPARTMENT OF ENERGY
MILESTONE SCHEDULE ☐ PLAN ☒ REPORT

FORM APPROVED
OMB 1901-1400

1. TITLE	2. REPORTING PERIOD	3. IDENTIFICATION NUMBER
ISOBUTANOL METHANOL MIXTURE FROM SYNGAS	April 1, 1996 - June 30, 1996	DE - AC22 - PC94PC066

4. PARTICIPANT NAME AND ADDRESS	5. START DATE	6. COMPLETION DATE
Department of Chemical Engineering University of California - Berkeley	Oct 1994	Sept 1997

7. ELEMENT CODE	8. REPORTING ELEMENT	9. DURATION	10. PERCENT COMPLETE a Plan	10. PERCENT COMPLETE b Actual
		94: O N D / 95: Q2 Q3 Q4 O N D / 96: J F M A M J J A S / 97: Q1 Q2 Q3 Q4		
	Task 4	Identify reaction intermediates by TPSR and high pressure infrared methods	40	30
	Tasks 3 & 5	Identify catalysts with highest isoalcohol yields (two) and evaluate at conditions resembling envisioned commercial practice.	40	15
	Task 5	Assess economic viability of these catalytic materials	0	0
	Task 5	Complete testing of at least two selected catalysts in slurry reactors.	0	0
	Tasks 3 & 5	Choose two materials for detailed studies of the reaction mechanism and of optimum synthetic protocols	0	0
	Tasks 3 & 5	Complete mechanistic studies on most promising materials	0	0
	Tasks 2 & 5	Develop synthetic procedures that can be carried out on a commercial scale Suggest a range of catalyst compositions for future study.	0	0
	Task 5	Complete testing of the two selected catalytic materials	0	0
	Task 5	Assess future research requirements, technical readiness and economic viability of the most promising approach	0	0
		Produce final report	0	0

1. TITLE ISOBUTANOL- METHANOL MIXTURE FROM SYNGAS					2. REPORTING PERIOD Apr. 1, 1996 to Jun. 30, 1996						3. IDENTIFICATION NUMBER DE-AC22-PC94PC066		
2. PARTICIPANT NAME AND ADDRESS Department of Chemical Engineering University of California- Berkeley, Berkeley, CA 94720					5. COST PLAN DATE Jul. 15, 1996						6. START DATE OCT 1994 7. COMPLETION DATE OCT 1997		
8. Element code	9. Reporting element	ACCRUED COSTS				ESTIMATED ACCRUED COSTS							
		Reporting period		Cumulative to date		a.total this	b. balance of	c. FY96	d. FY 97			12. Total contract	
		a. Actual	b. Plan	c. Actual	d. Plan	fiscal year	fiscal year	(1)	(2)	(3)	e. total	Value	13. Variance
	1. Total (Direct material)	9,174	22,777	69,027	142,374	44,234	46,875	91,109	94,782		210,684	259,929	49,245
	a) Purchased Parts	7,300	9,106	59,125	101,362	35,557	868	36,425	40,200		100,193	98,175	-2,018
	b) Subcontracted Items	1,856	13,670	3,970	115,052	3,970	50,709	54,679	54,582		109,261	161,754	52,493
	c) Other	18	0	5,913	74,043	4,708	0	0	0		5,913	0	-5,913
	2. Material Overhead	0	0	0	0	0	0	0	0		0	0	0
	3. Direct Labor Total	16,421	20,892	92,682	143,029	46,061	37,508	83,569	92,812		223,002	256,725	33,723
	4. Labor Overhead	0	0	0	0	0	0	0	0		0	0	0
	5. Fringe Benefits	1,828	3,350	10,794	22,818	5,468	7,932	13,400	15,368		34,094	41,538	7,444
	6. Special Testing	383	0	2,381	0	815	0	0	0		2,381	0	-2,381
	7. Special Equipment	1,988	2,000	287,968	258,000	43,790	-35,790	8,000	0		252,178	260,000	7,822
	8. Travel	0	1,629	5,882	11,091	3,694	2,821	6,515	7,020		15,723	19,740	4,017
	9. Consultants	0	0	0	0	0	0	0	0		0	0	0
	10. Other Direct costs	0	6,114	0	41,631	0	24,455	24,455	25,677		50,132	73,422	23,290
	11. Direct costs and Overhead	29,793	56,761	468,734	618,941	144,063	82,981	227,044	235,653		787,368	911,354	123,986
	12. General and Administrative Expense '49.5 %	13,875	20,505	90,090	145,252	50,036	31,984	82,020	90,358		212,431	256,108	43,677
	13. Facilities Capital Cost of Money	0	0	0	0	0	0	0	0		0	0	0
	14. Total Estimated Cost	43,668	77,266	558,824	764,192	194,099	114,963	309,062	326,008		999,795	1,167,462	167,667
	15. Fee	0	0	0	0	0	0	0	0		0	0	0
	16. Cost Sharing	1,603	9,949	205,766	242,902	17,011	22,786	39,797	56,789		285,341	301,651	16,310
	17. Total estimated DOE funds spent = Item 14-Item 16	42,065	67,316	353,058	521,290	177,088	92,177	269,265	269,219		714,454	865,811	151,357
14. Total		42,065	67,316	353,058	521,290	177,088	92,177	269,265	269,219		714,454	865,811	151,357

15. DOLLARS EXPRESSED IN	16. SIGNATURE OF PARTICIPANT PROJECT MANAGER AND DATE	17. SIGNATURE OF PARTICIPANT'S AUTHORIZED FINANCIAL SERVICE REPRESENTATIVE AND DATE
One U.S. Dollar		7/16/96 Lourdes Ferrer